BIOPHYSICS

Role of allosteric switches and adaptor domains in long-distance cross-talk and transient tunnel formation

Nandini Sharma[1], Navjeet Ahalawat[2]*, Padmani Sandhu[1]*, Erick Strauss[3], Jagannath Mondal[2], Ruchi Anand[1]†

Transient tunnels that assemble and disassemble to facilitate passage of unstable intermediates in enzymes containing multiple reaction centers are controlled by allosteric cues. Using the 140-kDa purine biosynthetic enzyme PurL as a model system and a combination of biochemical and x-ray crystallographic studies, we show that long-distance communication between ~25-Å distal active sites is initiated by an allosteric switch, residing in a conserved catalytic loop, adjacent to the synthetase active site. Further, combinatory experiments seeded from molecular dynamics simulations help to delineate transient states that bring out the central role of nonfunctional adaptor domains. We show that carefully orchestrated conformational changes, facilitated by interplay of dynamic interactions at the allosteric switch and adaptor-domain interface, control reactivity and concomitant formation of the ammonia tunnel. This study asserts that substrate channeling is modulated by allosteric hotspots that alter protein energy landscape, thereby allowing the protein to adopt transient conformations paramount to function.

INTRODUCTION

The allosteric regulation of function via long-distance interaction is a prevalent phenomenon, observed in several enzymes in biology (*1*–*3*). In some cases, effector molecules bind at a distal site and control reaction rates by altering the thermodynamics of the reaction coordinate (*4*, *5*). Both allostery and catalysis are rooted in the flexibility of the protein, which can give rise to an ensemble of conformational states (*3*, *6*). Consequently, the native state, instead of being viewed as a single low-energy minimum, can be considered to be a collection of quasi-degenerate states (*7*). Stimuli from substrates or allosteric effectors can temporarily shift the populations of these states either by orchestrating a major conformational change at the active site or through a subtle rearrangement of the network of interactions that permeate across, thereby favoring a particular conformation (*6*). These conformations can potentially be the major players in facilitating both catalysis and long-distance communication in proteins (*8*). These transient states that in this manner appear and disappear during the course of reaction are difficult to capture by conventional techniques; therefore, a combinatorial approach is required to characterize them.

For enzymes that transport unstable intermediates between active sites over a long distance, interdomain communication is triggered at specific locations, leading to the passage of the intermediate via tunnels (*9*). In such cases, there is a need to synchronize the reaction rates to facilitate subsequent chemical reactions at the distal site (*10*, *11*). To establish this fine control, specific gates that open and close in a timely fashion are instituted at strategic positions (*9*). Such molecular gates assist the transfer of labile intermediates by providing a privileged mode of selection across the length of the tunnel. The conduits regulated by these gates either can be preformed as in the case of carbamoyl phosphate synthetase (CPS) (*12*), imidazole glycerol phosphate synthetase (IGPS) (*13*), and pyridoxal phosphate (PLP) synthase (*14*) or can be transient as in phosphoribosylpyrophosphate amidotransferase (PPAT) (*15*) and glucosamine-6-phosphate synthetase (GlmS) (*16*).

Although preformed tunneling systems are well studied, information on transient channels remain rather scarce. These short-lived conduits are formed only during the time scale of the reaction (*8*), thus making their trapping in action a formidable task. To better understand the process of assembly and disassembly of these transient tunnels, here we have selected to study the bifunctional multidomain enzyme formylglycinamideribonucleotide amidotransferase (PurL), which is essential for catalyzing the fourth step of the purine biosynthesis pathway (Fig. 1A) (*17*). PurL has two active sites, separated by ~25 Å (Fig. 1B), a glutaminase site (G-site) where ammonia is released, and a formylglycinamidine (FGAM) synthetase site (F-site), where ammonia is transmitted and then incorporated into formylglycinamideribonucleotide (FGAR) in an adenosine triphosphate (ATP)–dependent fashion (*17*). On the basis of several considerations, this bifunctional enzyme is an excellent model system for exploring allostery and substrate channeling. First, PurL is intriguing as it has evolved to include an additional domain [N-terminal domain (NTD)] (Fig. 1B) along with peripheral gene-duplicated domains that appear to be essential for function (*17*). Second, PurL has an added layer of complexity, as it exhibits genetic plasticity, i.e., exists as an unusually large single polypeptide enzyme in humans and eubacteria (*17*) and as a three-protein complex in lower organisms (*18*). Such diversity makes PurL attractive from a drug design perspective, as this enzyme plays a central role in supplying precursors for the synthesis of DNA and RNA (*19*).

Previous studies on PurL have shown that ammonia production is significantly stunted in the absence of the substrate FGAR, indicative of the strong catalytic coupling between the G-site and F-site (*18*). Moreover, the available structure of PurL reveals that it is essentially trapped in an unproductive conformation with partial glutamine hydrolysis in the G-site (as evidenced by trapping of the covalent thioester intermediate) (Fig. 1B), and no apparent conduit connecting the two sites could be identified (*17*). Attempts to trap the enzyme in various steric states have so far been unsuccessful. Hence, to probe the mechanism of allosteric communication and to unravel

[1]Department of Chemistry, Indian Institute of Technology Bombay, Mumbai 400076, India. [2]Center for Interdisciplinary Science, Tata Institute of Fundamental Research, Hyderabad 500107, India. [3]Department of Biochemistry, Stellenbosch University, Stellenbosch 7602, South Africa.
*These authors contributed equally to this work.
†Corresponding author. Email: ruchi@chem.iitb.ac.in

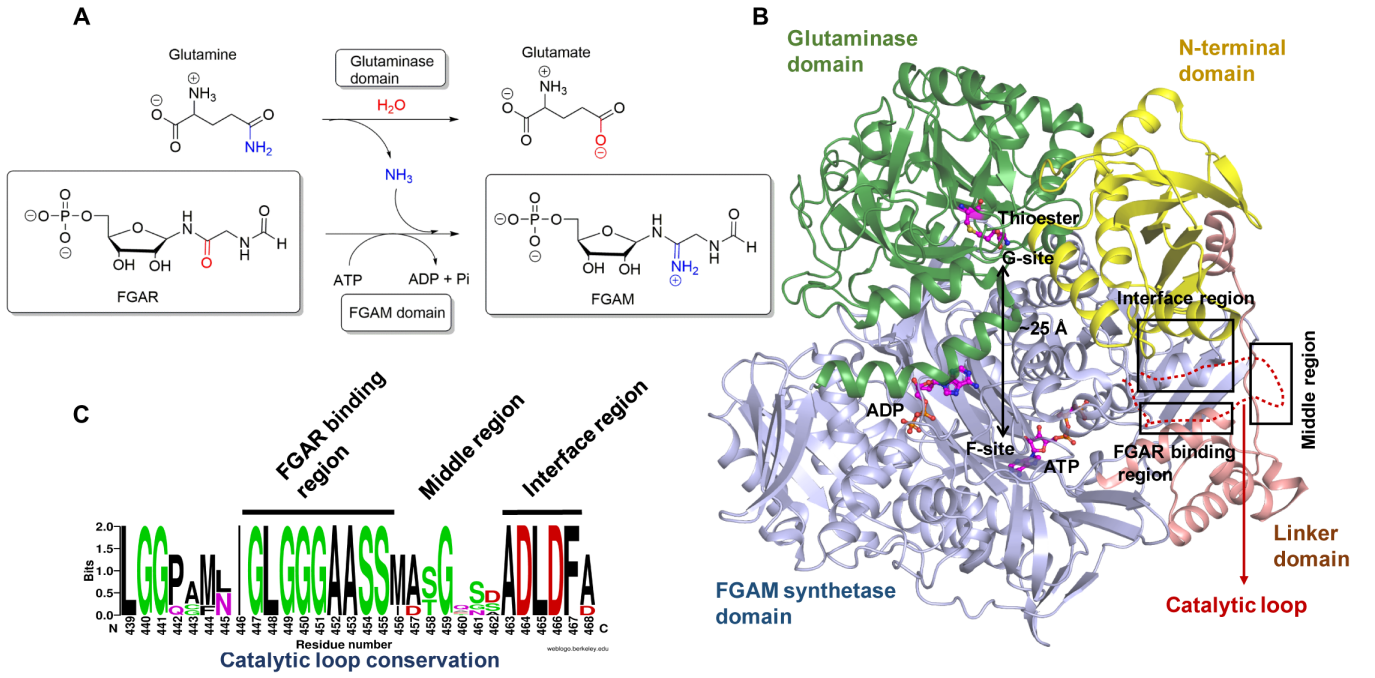

Fig. 1. Formylglycinamideribonucleotide amidotransferase (PurL). (**A**) Reactions catalyzed at both the active sites. (**B**) Domain organization of PurL. Carbon atoms of the glutamylthioester at the G-site and ATP at the F-site are depicted in magenta ball and stick structure. The disordered catalytic loop is shown by a red dotted line. (**C**) Conservation analysis of the C-loop residues, using 500 lgPurL (large PurL), found in eukaryotes and eubacteria sequences. The height of the letters depicts the degree of conservation.

the path followed by ammonia, we devised strategies to mimic the substrate-bound states of the enzyme. Using a combination of x-ray structure, enzymology, and molecular dynamics (MD) simulations, we reveal the origin of the allosteric switch. In addition, the conformational states of the enzymes were sampled to identify the state that captures the transient ammonia tunnel and help establish the mechanism of gating. Our results reveal the pivotal role played by the nonfunctional yet essential NTD in allosteric communication.

RESULTS

Identification of the allosteric switch

In several enzymes such as PPAT (*20*), IGPS (*21*), and GlmS (*22*), where long-distance communication occurs across the length of the protein, key allosteric switches have been identified, which seed the process of catalytic coupling. On the contrary, the identity of such a switch has remained elusive in the case of PurL. Analysis of the x-ray structure of lgPurL [Protein Data Bank (PDB) ID 1T3T] (Fig. 1B) revealed that it is trapped in a well-defined conformation. Electron density was visible for almost all of the 1295–amino acid residues except for the 22-residue-long catalytic loop (C-loop) that resides near the F-site (Fig. 1B) (*17*). In *Thermotoga maritima* (*23*), PurL exists as a complex of PurS, PurQ, and smPurL [respective homologs of NTD, glutaminase domain (GD), and FGAM synthetase domain (FD) of lgPurL] protein triad. In *T. maritima* smPurL, the C-loop, in the presence of FGAR, is known to adopt a defined secondary structure and serves as a cap, covering the F-site (*24*). Because strategically placed mobile loops have been attributed to be crucial for function in several systems (*25*), we hypothesized that the PurL allosteric switch might reside within this loop.

To delineate the plausible residues that partake in allostery, we first undertook the structure-based sequence alignment of the 22–amino acid C-loop region with 500 lgPurL sequences (see Materials and Methods). Two contiguous stretches bearing nearly 100% conservation score were identified, wherein the first region (447 to 451) is glycine-rich, while the second region (463 to 467) harbors bulkier amino acids (Fig. 1C). Both of these conserved regions were subjected to mutagenesis/truncations, and their effects on the enzyme's glutaminase, FGAM synthetase, and leaky (unproductive) ammonia activities were monitored. Our results show that the C-loop exhibits modularity in function. While deletion of the highly conserved glycine-rich stretch selectively impairs FGAM synthetase activity, it does not affect ammonia production (Table 1 and Fig. 2, A to C). In contrast, both enzymatic activities are highly correlated for the residues spanning the interface region (463 to 467) (Table 1 and Fig. 2, A to C). Progressive mutations in this stretch resulted in systematic reduction of glutaminase activity, with the triple mutant D464A_L465A_F467A (AS-3) exhibiting complete loss of bifunctional activity (Table 1 and Fig. 2, A to C; see also Supplementary Results and Discussion). Isothermal calorimetry (ITC) studies on these mutants suggested that reduction of glutaminase activity correlates to a diminishing glutamine binding ability upon going from AS-1 to AS-2 (Table 1, fig. S1, and table S1), with the triple mutant AS-3 exhibiting no affinity (Table 1 and Fig. 2D). These results indicate that the interface region of the C-loop, located ~30 Å away from the G-site, transmits a signal over long distance and is crucial for restructuring the G-site to a catalytically competent state.

To gain further insights into the conformations adopted by the C-loop, we determined the x-ray structures of various C-loop mutants (table S2). For protein variants, where mutations within the FGAR binding region (447 to 451) were performed, no major structural changes were observed as compared to the native state. In contrast, subtle variations in the active-site architecture were visible for the mutants that control allosteric communication (Table 1;

Table 1. Reaction profile of various PurL mutants. +++, maximum activity; ++, moderate activity; +, poor activity; –, no activity; ↓, less leaky than PurL; ↑, more leaky than PurL; ND*, not determined; NB**, no binding. Dissociation constant for each PurL mutant was determined via ITC; average values ± SD from two datasets were calculated using OriginPro 9.1 software.

Region of mutation	Proteins	Glutamate production	FGAM production	Leaky ammonia activity	Dissociation constant K_d (μM)
	Native PurL	+++	+++	–	2.3 ± 0.08
Allosteric switch	D464A (AS-1)	++	++	↓	5.4 ± 0.10
Allosteric switch	D464A-L465A (AS-2)	+	+	↓	29.6 ± 1.03
Allosteric switch	D464A-L465A-F467A (AS-3)	–	–	ND*	NB**
FGAR binding region	450-451_del (Δ1)	+++	–	↑	7.1 ± 0.11
FGAR binding region	452-453_del (Δ2)	++	–	↑	18.9 ± 0.93
Middle region	458-462_del (Δ3)	++	++	↓	16.9 ± 0.76
N-term interface	R80A (NAS-1)	++	++	↓	15.6 ± 0.88
N-term interface	R134A-M135A (NAS-2)	++	++	↓	11.0 ± 1.21
N-term interface	R80A-R134A-M135A (NAS-3)	–	–	ND*	NB**

Fig. 2, A to C; and fig. S2). For instance, in the D464A (AS-1) mutant, the key catalytic residues and structured active-site water molecules at the F-site become disordered (fig. S2), although its overall conformation is similar to that of the wild type. This flexibility is indicative of a more solvent-exposed active site (see Supplementary Results and Discussion). In contrast, the active-site architecture is restored for the double mutant D464A_L465A (AS-2) (fig. S2), and even the dynamic C-loop, which is found to be disordered in all previous structures, adopts a defined conformation (Fig. 2E). For this scenario, the C-loop residues 451 to 455 fold into a 3_{10} helix and residues 461 to 467 adopt a helical conformation. A comparison of the C-loop conformation with the previously determined structure of the FGAM synthetase fragment of TmPurL (Fig. 2F) (*24*) shows that the C-loop conformation in the double mutant essentially mimics that of the FGAR-bound state. Moreover, in the catalytically compromised AS-2 variant, the unreacted glutamine substrate, rather than the usual glutamylthioester intermediate, was captured in the G-site (Fig. 2G). Therefore, by introducing appropriate mutations, we were able to substantially slow down the reaction rates and successfully trap the enzyme in a conformation, where both substrates are bound to their respective sites, a state primed for allostery.

Mechanism of allosteric communication

MD studies were carried out to identify the conformational states that lead to allostery and channel formation. Starting from the closed state of the C-loop captured via x-ray crystallography, multiple 1-μs simulations were carried out in the presence and absence of glutamine. Analysis of trajectories in the presence of glutamine shows that the C-loop shuttles between three major conformational states: (i) completely closed, (ii) partially open, and (iii) fully open (Fig. 3A and fig. S3A). MD results for the apo state reveal that the C-loop adopts a closed conformation over the length of the simulation (fig. S3A), exhibiting no significant allosteric conformational changes. To examine the impact of the C-loop conformations on the overall enzyme structure, we analyzed correlations of fluctuations of Cα atoms along the trajectories. The majority of the correlations (generalized correlation coefficient, $r_{MI} > 0.8$) in the apo state are present as self-correlated motions (fig. S3B), suggesting a lack of cross-domain communication. On the other hand, in the glutamine-bound form of the enzyme, C-loop residues were found to be highly correlated with those of the other three domains (Fig. 3B). Because global structural changes are observed only in a state that mirrors the presence of a substrate in both the active sites, we conclude that the presence of reactants in both the sites is a prerequisite for catalytic coupling.

To determine the modes that are likely to exhibit biologically relevant global motions, we performed principal component analysis (PCA) on glutamine-bound trajectories. The first eigenvector with largest eigenvalue (fig. S3C) was chosen as the principal mode, and the two-dimensional projection of protein motion on phase space along eigenvectors 1 and 2 was plotted (fig. S3D). Root mean square fluctuations calculated for the backbone residues (fig. S3E) showed that the most significant motions occur in the trajectories in which the C-loop is in a partially opened conformation. In these poses, the NTD, linker domain, and G-site undergo substantial motions (Fig. 3C and fig. S3E). In addition, MD trajectories reveal that as the C-loop starts to adopt an open conformation, it begins to interact with the glove-shaped NTD (Fig. 4A). The interaction with the C-loop induces a ~8° rotation in the NTD, in the forward direction, toward the FD, pulling it away from the GD. As seen from the 570-ns snapshot (Fig. 4, B and C), the interfacial region of the C-loop starts to communicate via a mixture of hydrogen bonding and van der Waals interactions with the NTD residues, residing in

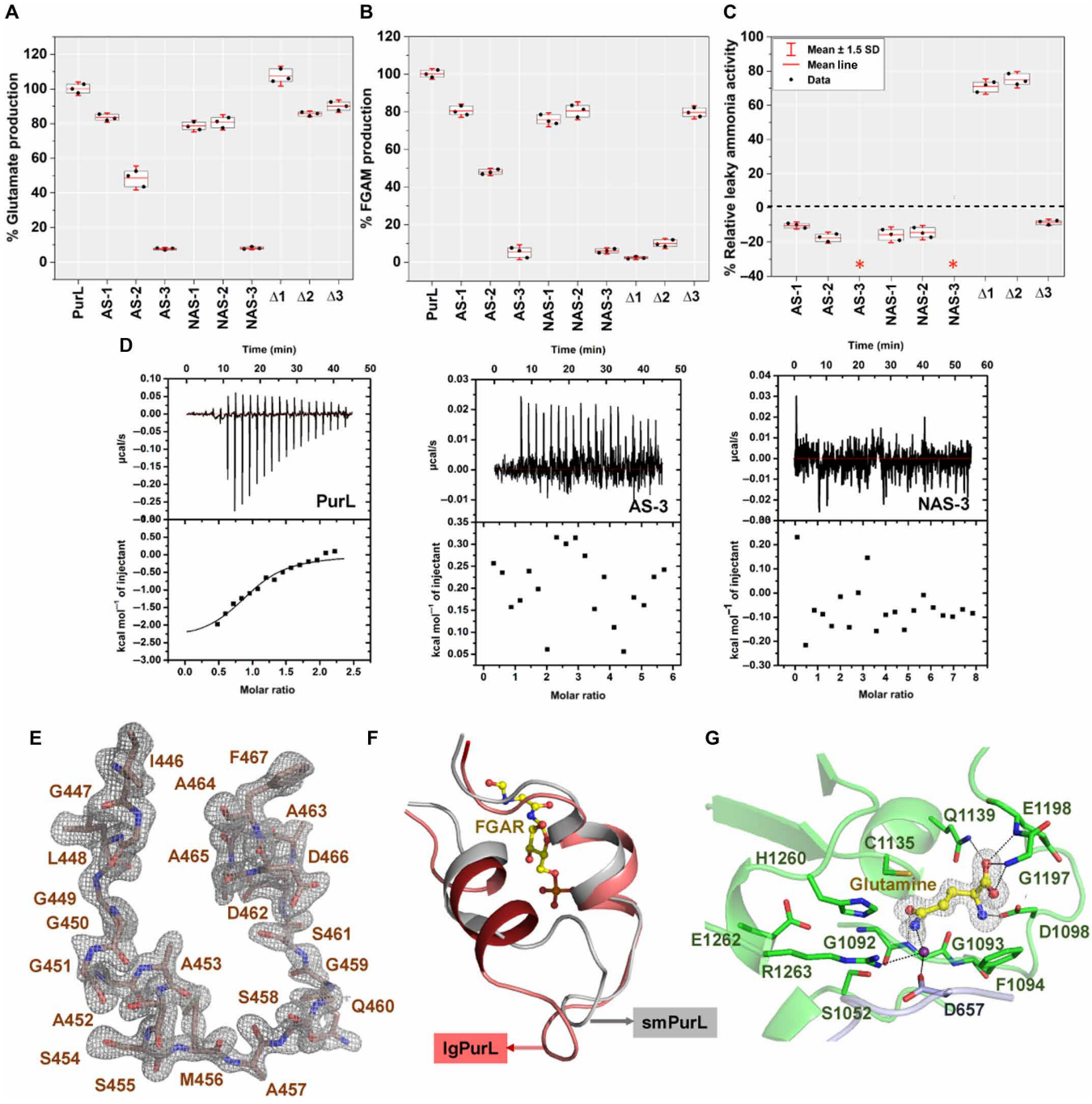

Fig. 2. Activity assay and binding profile of various PurL mutants and x-ray crystallography analysis of the AS-2 mutant. (**A**) Glutaminase activity, (**B**) FGAM activity, and (**C**) leaky ammonia activity expressed as percentage relative to that of wild-type enzyme. Asterisks represent no unproductive release of ammonia, as no glutamate production was observed. (**D**) Glutamine binding profile for PurL, AS-3, and NAS-3. Data obtained for each titration were fitted into one set of sites model and analyzed using OriginPro 9.1. (**E**) mFo-DFc electron density map of the C-loop. (**F**) Superposition of the ordered C-loop of AS-2 (labeled as lgPurL) with that of TmPurL (labeled as smPurL). The FGAR structure is represented by ball and stick. (**G**) Trapped glutamine molecule in the G-site. For the ligands shown in the ball and stick model, the carbon, oxygen, and nitrogen atoms are in yellow, red, and blue, respectively. The violet sphere represents a water molecule, which forms bridging hydrogen bonds with glutamine. The mFo-DFc electron density maps were contoured at 3.0 σ.

the loop connecting α3 and β3 (topology numbered in accordance with native PurL). The interfacial C-loop also establishes an interaction interface with the β5 and α4 region of the NTD (Fig. 4, B and C). In brief, M444, V470, and F467 in the C-loop together form a hydrophobic network, with residues R134, M135, M136, and I84 present in the NTD (Fig. 4C). Moreover, R80 from the NTD anchors onto the C-loop via hydrogen bonding interactions (Fig. 4C). The probability distribution obtained from the MD trajectories shows that

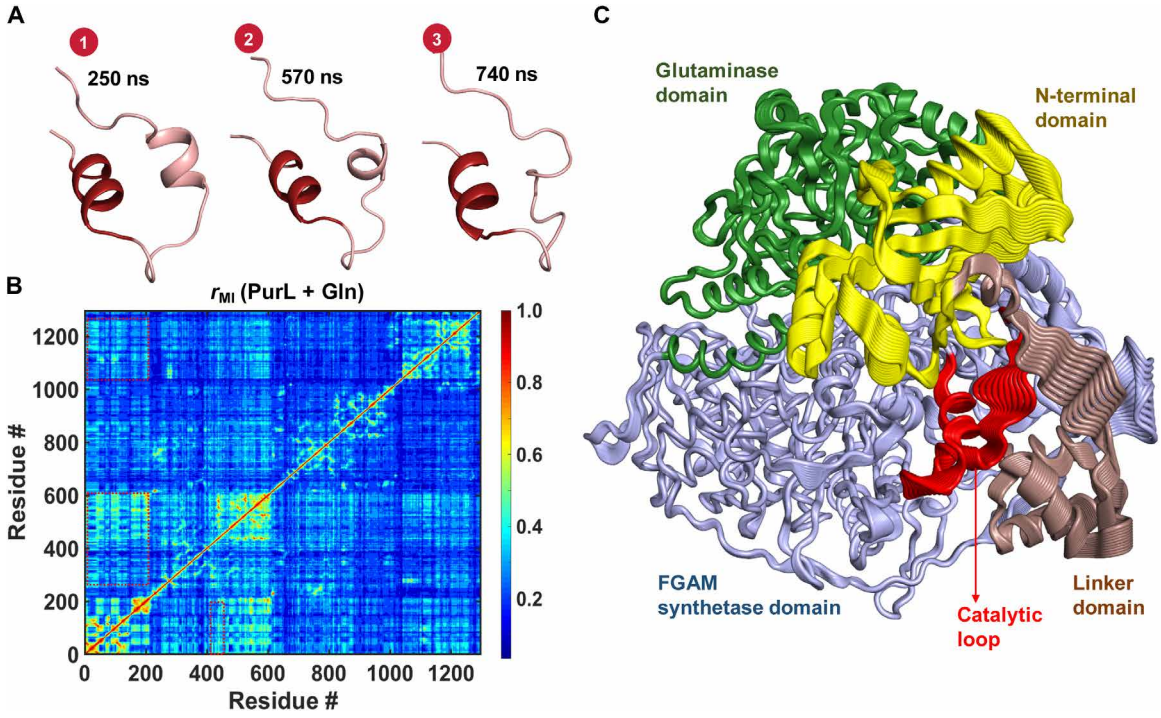

Fig. 3. MD and PCA. (**A**) Three major conformations adopted by the C-loop: 1, completely closed; 2, partially open; and 3, fully open. Location of the allosteric switch is highlighted using dark red color in the C-loop. (**B**) r_{MI} plot for glutamine-bound PurL. Red dotted boxes represent the correlated regions in PurL. (**C**) Global motions depicted in PurL based on PCA.

these contacts are maintained for a substantial duration (fig. S4, A and B).

The newly formed C-loop/NTD communication network seeds allosteric communication in lgPurL, and the contacts created consequently facilitate transmission of the information to the G-site (Fig. 4D). The swinging motion of the NTD triggers substantial rearrangement at the C-loop/NTD interface, leading to the reorganization of the ternary interface (created between NTD, GD, and helix α13). This induces restructuring of several hydrogen bonds and hydrophobic interactions (Fig. 4, E and F). That is, interactions along the NTD/GD interface formed by residues L59, K90, I94, and N97 of the NTD and 1096 to 1100 stretch from the GD are disrupted (Fig. 4, E and F). These movements help open a passage between the two domains and facilitates the entry of glutamine to the G-site (Fig. 4C). The most significant conformational change observed at the NTD/GD interface is the release of the "oxyanion strand," a recurring feature in almost all amidotransferases that is responsible for the stabilization of the anionic transition state (scheme S1) (*26*). The conformational change induces a disruption of the hydrogen bonding interaction of G1092 on the oxyanion strand with N1051, which resides near the GD active-site entrance (Fig. 4, E and F). The release of this residue imparts flexibility and aids in the creation of the "oxyanion hole," which facilitates glutamine hydrolysis. On the basis of the above analysis, we conclude that the information initiated via allosteric switch controls the activation status of the G-site. Essentially, the NTD acts as a bridge. On one side, it interfaces with the reaction site where ammonia is released; while on the other side, it interacts with the F-site. Further, we observe that the NTD influences substantial rearrangement of the linker domain (fig. S5) and the auxiliary adenosine diphosphate (ADP) binding loop (fig. S5) and triggers the conformational changes that percolate across the entire structure (see Supplementary Results and Discussion). Thus, multiple lines of evidence corroborate that the C-loop is the initiator site, where allosteric communication is seeded, while the NTD is the focal domain that interfaces with various regions of the protein, thereby transmitting appropriate signals.

Formation of the transient ammonia channel

The identity of the ammonia tunnel has been a long-standing debate, and as of yet, the path describing the transport of ammonia has not been fully characterized. While analyzing MD trajectories, we noted that the partially open C-loop state that partakes in the transmission of the allosteric signal also harbors a fully formed ammonia channel (Fig. 5A). In the MD snapshots (Fig. 5A), we visualize that transient tunnel formation occurs due to the overall motion of the secondary structural elements β12, β13, α10, α11, and α12 that form the walls of the channel (Fig. 5A). Residue A384 in the loop preceding β13 moves out of the channel path along with β12 residues V333 and F335. In addition, residue S312 on helix α11 and residues P370, A374, and N378 on helix α12 undergo substantial motion to facilitate channel formation. To further verify the MD results and confirm that the tunnel is formed via movement of these residues, we reanalyzed our previous experiments (*27*). Amino acids such as A384, V333, and S312 have previously been mutated, purified, and tested for both FGAM and glutaminase activities. The results (fig. S6, A to D) show that these residues play a central role in maintaining channel integrity. These channel-lining residues are very sensitive to perturbation, and drastic changes via mutations are not tolerated. Moreover, mutations that result in partial blocking of the path have a marked effect on channeling efficiency (*27*). For example, both

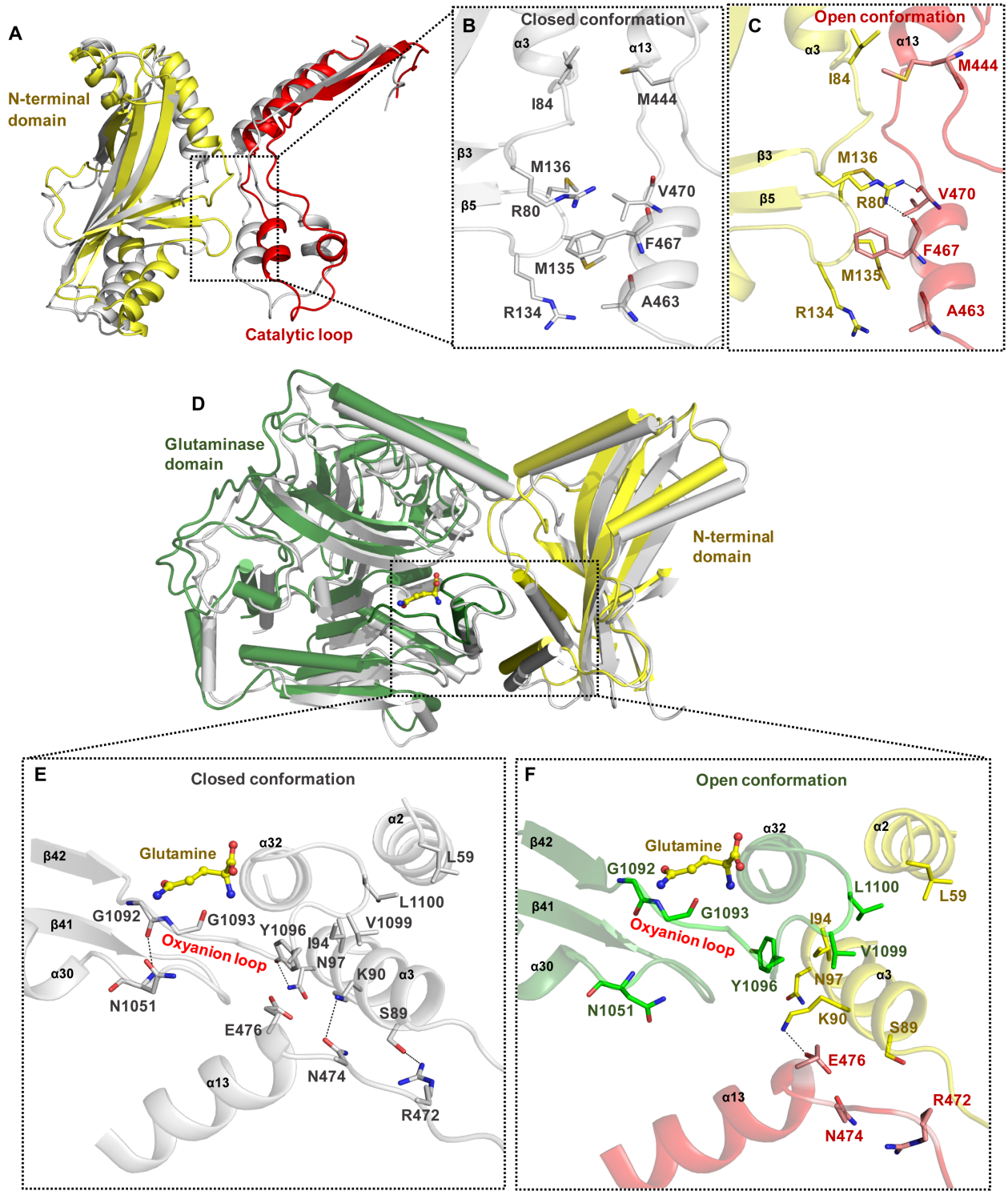

Fig. 4. Role of the NTD in allosteric signal transduction and oxyanion hole formation. (**A**) Superposition of the AS-2 crystal structure depicting the C-loop in the closed conformation (gray) with the glutamine-bound MD snapshot. Zoomed views of the interface region in the inset show (**B**) the crystal structure of the AS-2 mutant (the closed conformation) and (**C**) the MD snapshot (the open conformation). (**D**) Superposition of the AS-2 crystal structure with the glutamine-bound MD snapshot. Zoomed view of the NTD/GD/C-loop interface, with inset (**E** and **F**) depicting the closed conformation of AS-2 PurL and the MD snapshot, respectively. The NTD is shown in yellow, the oxyanion loop from GD is shown in green, and the C-loop that is downstream from the FGAM domain is shown in red. Glutamine is represented by a ball and stick model, with carbon, oxygen, and nitrogen atoms in yellow, red, and blue, respectively.

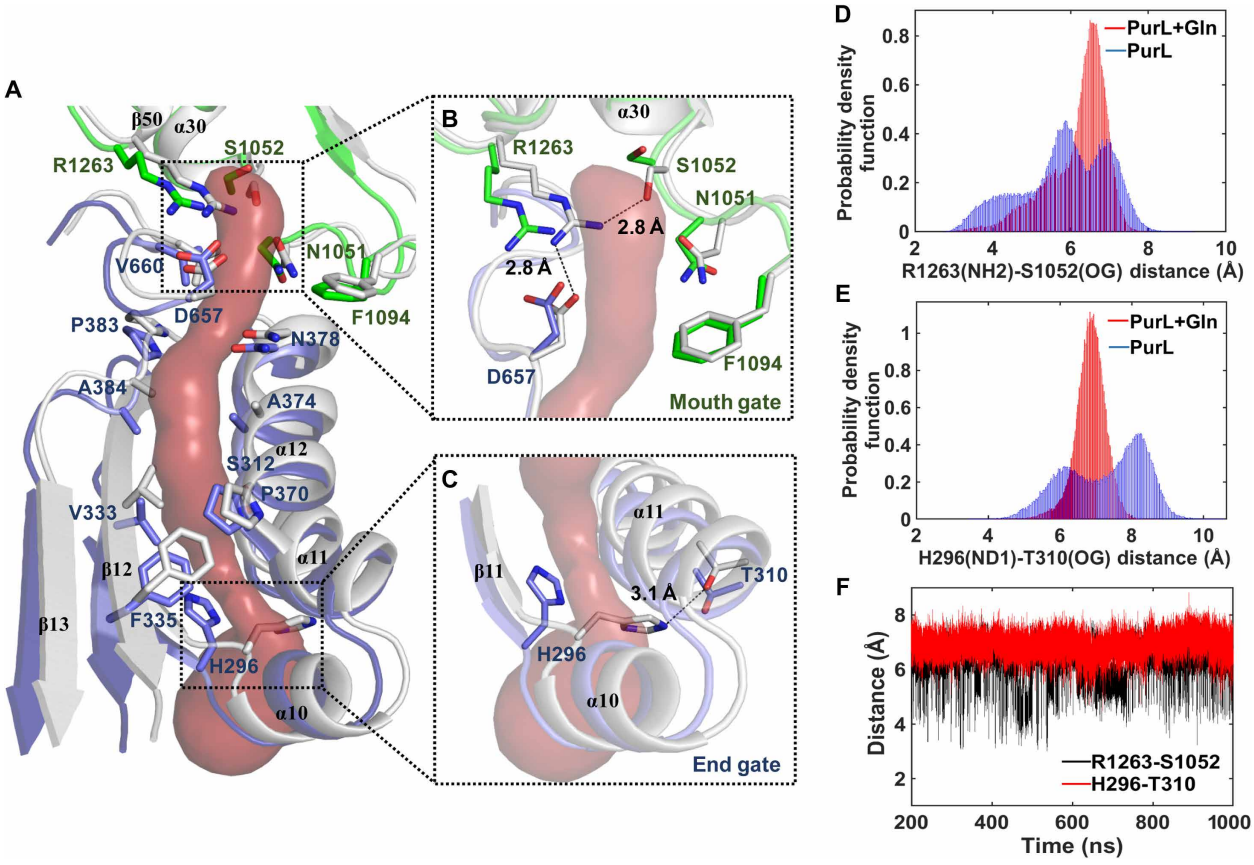

Fig. 5. Transient ammonia tunnel. (**A**) Superposition of the 570-ns glutamine-bound MD snapshot, with the crystal structure depicting fully formed ammonia tunnel (identified using CAVER 3.0 PyMOL plugin). The portions shown in green and blue belong to GD and FD, respectively. The insets show the zoomed view of (**B**) the mouth gate and (**C**) the end gate. Distance probability density plots of (**D**) the mouth (entrance) gate and (**E**) the end gate in the apo and glutamine-bound simulations are plotted. (**F**) Distance between key gating residues [R1263(NH2)-S1052(OG)] and [H296(ND1)-T310(OG)] over the course of the simulation, indicating that end gate remains open but mouth gate opens and closes.

crystallography and biochemical assays (fig. S6, A to D) show that the V333I mutant constricts the channel by ~2 Å. This leads to enhance the leakage of ammonia and decreases the FGAM synthetase activity. All these experimental evidences strengthen our proposal that the tunnel formation revealed by the simulation studies reflects a true biological representation of the event.

It was additionally identified that two gating switches (Fig. 5A) primarily govern the passage of ammonia: one at the mouth (entrance) of the channel, consisting of residues R1263, S1052, D657, and N1051, and the other at the end (exit), constituted by residues H296 and T310. Comparison of the MD pose with the crystal structure revealed a rearrangement of the hydrogen bonding network between R1263, S1052, and N1051 (Fig. 5B). Outward swinging of the R1263-D657 salt bridge and concomitant flipping of the hydroxyl group of S1052, away from the entrance, open the gate (Fig. 5B). At the end of the channel, the ammonia access is blocked by the H296 residue (Fig. 5C). FGAR binding induces H296 to flip out of the channel, breaking its interaction with T310, thereby opening the end gate (Fig. 5C). In this manner, the passage of ammonia is facilitated when both of the gates are open. Distance probability plots (Fig. 5, D and E) corroborate the above observation and show that, for the glutamine-bound state, both the gates remain open with a higher probability compared to the apo state.

The key questions that arise at this juncture are the following: What is the driving force that facilitates opening and closing of the channel, and which gate is likely to open first? Analysis of the distance plot as a function of time (Fig. 5F) revealed that while the end gate remains open for a longer period, the mouth gate shuttles between open and closed forms. A corroborating frustration index (FI) (*28*) analysis shows that the gate at the end of the channel is in a highly frustrated conformation, whereas residues at the mouth gate are in a much more relaxed conformation (fig. S6, E and F). The opening of the end gate lowers the FI at this position, while it increases the FI at the mouth gate (fig. S6, G to J). Therefore, it can be concluded that the gating is controlled at the F-site, i.e., the information is first transmitted from the F-site to start the catalytic cycle with the communication seeded via the motions in the C-loop.

Experimental validation of the role of NTD in catalytic coupling

To validate MD predictions, we progressively mutated the NTD residues that form the dynamic C-loop/NTD interface (Fig. 4C). The NTD variants were constructed, purified, and tested to determine the effects on both FGAM synthetase and glutaminase activities (Fig. 2, A and B). We find that the progressive disruption of the C-loop/NTD interface leads to a marked reduction in both ammonia production

and FGAM synthetase activities (Table 1 and Fig. 2, A and B). For the case of the triple mutant R80A_R134A_M135A (NAS-3), where the NTD interactions with the C-loop are disrupted, neither glutaminase nor FGAM synthetase activities were observed (Table 1 and Fig. 2, A and B). Therefore, it is evident that disruption of the interfacial region by either making allosteric switch mutations in the C-loop or in the NTD residues it contacts results in stunted ammonia production (Table 1 and Fig. 2A). We observe a similar effect for the NTD mutants with respect to their ability to bind glutamine (Table 1; table S1; and fig. S1, F and G). With each successive mutation, the capacity of the mutant enzyme to bind glutamine is compromised, similar to that noted with the C-loop mutations (Table 1, table S1, and fig. S1). These observations imply that the disruption of the NTD interface impedes proper passage of the allosteric signal. It is likely that the polar path that serves as the entry and exit for glutamine/glutamate moiety (fig. S4C) is only effectively created upon passage of appropriate signal. Overall, these experiments reassert that the dynamic C-loop/NTD interface interaction controls the entire reaction cycle in this bifunctional enzyme.

DISCUSSION

Multifunctional enzymes with multiple domains represent an evolutionary departure from the simple single-substrate enzymes (*29*). Enzymes that channel ammonia particularly form a class of complex systems that exhibit conformational plasticity. The control of ammonia production is allosterically governed via a shift in populations, directed by appropriate cues. What is striking in terms of both allosteric control and channel formation is that PurL presents several unique features. While the origin of the allosteric switch is similar to that of PPAT (*15*) and guanosine monophosphate (GMP) synthetase (*25*), the mechanism of signal transmission is distinct in PurL. In PPAT and GMP synthetase, the process of channel formation is direct, and rearrangement of the C-loop is responsible for the creation of the channel via a conformational change of the switch residues (*15*, *25*). In contrast, in PurL, allosteric control is mediated by the glove-like NTD, which acts as a bridge between the G-site and the F-site. In addition, the signal is primarily propagated through the interactions mediated via the NTD. It is the subtle motions in the C-loop that permeate to the NTD, initiating a cascade of correlated motions that alter the interaction networks, leading to the formation of the ammonia tunnel. An indirect mode of communication, where additional domains are introduced for control, has also been observed in GltS (*30*). In this case, the channel is not transient but is blocked at both ends, and changes in the bridging domain govern allostery (*30*).

Despite the focal role in synchronizing cross-talk, the adaptor NTD is highly variable and exhibits less than 10% sequence conservation between the single polypeptide eukaryotic and bacterial three-component PurLs (*17*, *23*). A close examination reveals that while the catalytic residues in the C-loop remain conserved, the interfacial residues that participate in allosteric communication are divergent in both the single and ternary component PurL systems (Fig. 1C and fig. S7). The question thus arises whether different modes of allosteric communication occur across species or if a common mechanism of transmission is followed. Analysis of diverse protein sequences shows that sequence heterogeneity is accounted by retaining a highly correlated set of residues along the C-loop and NTD interface, and this region coevolves as a unit across species. This type of diversity is not uncommon, and in several enzyme systems, the protein-protein interfaces coevolve to keep the overall relay similar, while the catalytic residues remain resistant to evolution (*31*). This mode of selection promotes conservation of the reaction mechanisms and simultaneously encourages species selectivity via promotion of unique communication interfaces. Because PurL is a key enzyme for survival in all organisms, the divergence can potentially be exploited toward targeted drug design. In this context, the selective blocking of the variable allosteric interface presents a viable strategy that can be explored for targeted inhibitor discovery.

Another significant finding that emerged through our study is the dual gate control for ammonia release. To ensure that the wasteful production/passage of intermediates is minimized, the presence of appropriate gating residues is commonly observed in several tunneling enzymes (*12*, *13*, *30*). Gates can be found in the middle of the channel, such as in CPS (*12*) and GlmS (*22*), or at the entry or exit points like in CTP (*32*) and IGPS (*33*). Dual gates are found only in systems where stringent control of enzyme performance is paramount, like in GltS (*30*). Because PurL catalyzes a key step in the de novo synthesis of the purines, its catalytic activities have been carefully modulated to achieve optimal efficiency through a dual gating control. Moreover, the gating action in PurL is coupled with active-site rearrangement. This type of gating control is reminiscent of IGPS (*21*), where the orientation of the oxyanion hole is primed for stabilization of transition state only when appropriate signals are received.

The question that remains a matter of debate is what directs the development of transient tunnels versus preformed conduits in an enzyme. It appears that the presence of gates along with transient tunnel is predominant in a system, where passive transport of substrates occurs across distal sites. We believe that the rate-determining step in PurL is the activation of the G-site with simultaneous assembly of a transient hydrophobic tunnel that enables passive transport of ammonia. This scenario is unlike the facilitated diffusion and active export of ions and water by membrane transport channels. For instance, in membrane-embedded ammonia transporters (*34*), ammonia is directed along the path, as an ammonium moiety via a protonation/deprotonation mechanism, and is finally released back as a nucleophilic ammonia moiety. It can therefore be concluded that a plethora of channeling systems has evolved according to functional needs, and the enzymes are tailor-made to exert excellent control at various levels. In some systems, the expense of facilitating functional stringency is borne at the cost of introducing large adaptor domains. Overall, the elegant allosteric control demonstrated here is proof of how subtle, yet accurate, interplay of molecular interactions governs important outcomes in biological systems.

MATERIALS AND METHODS

Sequence conservation analysis

Structure-based sequence conservation was analyzed using ConSurf online server available at http://consurf.tau.ac.il (*35*). Potential homologs of lgPurL (using PDB ID 1T3T) and smPurL (using PDB ID 2HS4) were extracted from the UniProt database using HMMER, a default search algorithm in ConSurf server, assigning *e*-value cutoff of 10^{-3} and by performing three iterations. Maximum 500 homolog sequences were selected and aligned using CLUSTALW by assigning a maximum 95% and a minimum 35% sequence identity as the cutoff. Last, the conservation score was calculated using the Bayesian method. On the basis of the structure of the ordered C-loop in TmPurL

(smPurL) crystal structure, the C-loop in lgPurL is divided into three sections. A conserved region, residues 449 to 455, is termed "FGAR binding region" due to its proximity to FGAR binding site. The region consisting of bulkier conserved residues, proximal to the NTD, is named "interface region." The "middle region" of the C-loop was found to be unconserved.

Cloning, expression, and purification

All mutants were constructed following the method of overlap extension polymerase chain reaction. Native PurL plasmid was used as a template for gene amplification using Phusion high-fidelity DNA polymerase. Amplified genes were ligated into pET-28a by using Kpn I and Bam HI restriction site and into modified versions of pET vector by using Bam HI, and Xho I restriction site. All mutants were transformed, then expressed in BL21_(DE3) cells, and finally purified as described previously (*36*). In brief, the starter culture was made by adding a single colony from transformed plasmid in BL21_(DE3) cells, grown overnight at 37°C, in 10 ml of LB media containing kanamycin (35 μl/ml). Two liters of LB media was inoculated with 10 ml of saturated starter culture and incubated at 37°C. When the culture reached an optical density (OD) of approximately 0.6, the temperature was lowered to 25°C, and cells were induced with 0.3 mM isopropyl-β-D-thiogalactopyranoside for 8 hours. After the cells were harvested by centrifugation at 5000 rpm for 15 min, the pellet was stored at −80°C. The pellet was resuspended in 25 ml ice-cold lysis buffer (50 mM 4-(2-hydroxyethyl)-1-piperazineethanesulfonic acid (HEPES), 500 mM NaCl, 1 mM imidazole, 1 mM L-glutamine, 5 mM $MgCl_2$, pH 7.5). Cells were lysed by sonication, and cell debris was removed by centrifugation at 14,000 rpm for 45 min. The supernatant of the protein solution was mixed with Ni–nitrilotriacetic acid resin (Qiagen), which was pre-equilibrated in lysis buffer and incubated for 1 hour. The supernatant was separated by centrifugation at 1200 rpm for 20 min. Nonspecific bound proteins were removed by extensive washing with wash buffer (50 mM HEPES, 500 mM NaCl, 5 mM Imidazole, 1 mM L-glutamine, 5 mM $MgCl_2$, pH 7.5). The His-tagged protein was eluted with the elution buffer (50 mM HEPES, 200 mM NaCl, 100 mM imidazole, 1 mM L-glutamine, 5 mM $MgCl_2$, pH 7.5). The eluted protein was further dialyzed in dialysis buffer (20 mM HEPES, 50 mM NaCl, 1 mM L-glutamine, 5 mM $MgCl_2$, pH 7.5) to remove imidazole. The purity of the protein was verified by running a 10% polyacrylamide gel followed by Coomassie blue staining.

Glutamate production

A reaction mixture with a total volume of 50 μl was set containing 20 mM phosphate buffer (pH 8.0), 20 mM $MgCl_2$, 80 mM KCl, 5 mM L-glutamine, 10 mM ATP, 2 mM FGAR, and 2 μM test enzyme according to the previously reported protocol (*37*). After 30 min incubation at 37°C, the reaction mixture was quenched by placing it in boiling water for 5 min. Subsequently, it was cooled on ice, and the reaction mixture was centrifuged and transferred into another vial to remove the precipitates. Glutamate production was monitored via a coupled standard glutamate dehydrogenase assay by measuring the reduction of 3-acetylpyridine adenine dinucleotide at 363 nm (*38*).

FGAM production

FGAM production was determined using a previously reported protocol (*37*). In brief, FGAR to FGAM conversion by PurL was coupled with PurM enzyme, which further converts FGAM to aminoimidazole ribonucleotide (AIR). A reaction mixture of 100 μl with 20 mM HEPES buffer (pH 7.5), 20 mM $MgCl_2$, 80 mM KCl, 50 mM L-glutamine, 10 mM ATP, and 500 μM FGAR with 5 μM PurL and 5 μM PurM enzyme was incubated at 37°C for 20 min. The reaction was quenched by adding 25 μl of 20% trichloroacetic acid (pH 1.4). Precipitates were removed by centrifugation. AIR product formation was determined by standard Bratton-Marshall's assay (*39*). The intensity of pink color observed was recorded at 500 nm using the SpectraMax M5 plate reader.

Leaky ammonia production

To measure the leaky (unproductive) ammonia activity, previously reported method was used (*27*). The reaction mixture mentioned above for glutamate production, containing 1 μM of the test enzyme, was supplemented with ammonia assay reagent [containing a mixture of α-ketoglutarate and NADPH [reduced form of nicotinamide adenine dinucleotide phosphate ($NADP^+$)] and with L-glutamate dehydrogenase enzyme provided in the ammonia assay kit from Sigma-Aldrich. NADPH oxidation to $NADP^+$ was monitored by recording the absorbance at 340 nm.

Isothermal calorimetry

To determine the binding affinity of PurL mutants with respect to substrate glutamine, ITC experiments were performed using MicroCal iTC_{200} (GE Healthcare). Protein of specified concentration (table S1) in a buffer (20 mM HEPES, 50 mM NaCl, and 5 mM $MgCl_2$, pH 7.5) was titrated against a specified concentration of L-glutamine in the same buffer at 25°C. For each titration, differential potential change was measured by injecting 2-μl volume of the titrant for 5 s. To obtain the optimal saturation curves, a total of 20 injections at an interval of 120 s were performed with a constant stirring rate of 1000 rpm throughout the titration. To nullify the effect of the heat of dilution, the ligand (L-glutamine) was titrated against the blank buffer and the data obtained were subtracted from the raw data of their corresponding protein-ligand titrations before model fitting. Data obtained from each titration were fitted to one set of sites model and analyzed using OriginPro 9.1. All titrations were repeated twice, and thermodynamic parameters and SDs were determined. The concentration of protein was calculated by measuring absorbance at 280 nm in ultraviolet-visible spectrophotometer using a molar extinction coefficient of 145,605 M^{-1} cm^{-1}.

CD spectroscopy

To determine the secondary structure content of various PurL mutants, a JASCO J-815 circular dichroism (CD) spectrometer was used. A 3.5 μM concentration of all the mutants (in phosphate buffer containing 50 mM sodium phosphate, 50 mM NaCl) was used for recording the spectra as reported previously (*36*). Scans were performed at 25°C using 0.1-mm path length quartz cuvette at a differential integration time of 8 s with a scan rate of 50 nm/min. Baseline corrections were performed before recording the spectra for all the mutants.

Crystallization, data collection, and refinement

Crystals for the mutants AS-1, AS-2, Δ1, and Δ2 were obtained by hanging drop vapor diffusion method at 298 K in 2 M $(NH_4)_2SO_4$. Datasets for the mutant AS-1, Δ1, and Δ2 were collected at the home source of Indian Institute of Technology (IIT) Bombay using

a Rigaku MicroMax-007HF x-ray diffractometer with a Rigaku R-AXIS IV++ detector. Frames were indexed, integrated, and scaled in $P6_5$ space group in HKL2000 (*40*). Crystal of the mutant AS-2 was diffracted at beamline ID29 using a PILATUS detector at the European Synchrotron Radiation Facility, Grenoble, France. Datasets were indexed, integrated, and scaled in $P6_5$ space group in XDS (*41*). Phases were generated, and structures were determined by performing molecular replacement in Phaser (*42*) and Auto-Rickshaw (*43*) against the published structure of native PurL (PDB ID 1T3T). Structure models were subjected to rigid body refinement and further refined using several cycles in REFMAC5 (*44*) in CCP4i suite (*45*). Manual model building was performed with WinCoot (*46*). Crystallographic data statistics are reported in table S2.

Modeling and MD simulations

The computational structural models were based on the crystal structure of AS-2 mutant of PurL in complex with glutamine, solved to a resolution of 1.7 Å with a closed (ordered) conformation of the C-loop. For apo simulations, the coordinates of glutamine ligand were removed from this crystal structure. All the crystal water molecules were removed, and the auxiliary ADP molecule was retained in both apo and glutamine-bound forms. The mutated residues at 464 and 465 positions in the C-loop were replaced back with the original residues of the native PurL. CHARMM27 (*47*) force field with CMAP correction was used to model the system implemented in GROMACS 5.1.2 package (*48*). The systems were solvated using the TIP3P (*49*) water model, and 51 Na^+ ions were added to neutralize the charge. The energy minimization was carried out using the steepest descent algorithm. The equilibration of the systems was performed in three steps: (i) a 500-ps NVT (constant particle number, volume, temperature) equilibration keeping 1000 kJ mol^{-1} nm^{-2} position restraint on all heavy atoms of protein and ligands using the Berendsen (*50*) coupling with a coupling constant of 0.1 ps at 310 K, (ii) a 1-ns position restrained equilibration under constant pressure and temperature condition (NPT) using the v-rescale (*51*) temperature coupling with a coupling constant of 0.1 ps and at 1 bar pressure with Parrinello-Rahman (*52*) pressure coupling with a coupling constant of 2.0 ps, and (iii) a 5-ns NPT equilibration without any restraints at 310 K with the same parameters as mentioned in step (ii). The independent production runs (1 μs each) with different initial velocities were performed under NPT ensembles using the same parameters as mentioned in step (iii).

Correlation analysis

Correlation analysis is a quantification of correlated motion in protein residues using the covariance matrix (*53*). We analyzed the correlated atomic fluctuations of amino acid residues using g_correlation tool (*54*). The correlation was calculated using mutual information–based generalized correlation coefficients (*54*), which do not depend on the relative orientation of the atomic fluctuations and can capture nonlinear correlations. The generalized correlation coefficient is a variation of linear correlation method, i.e., Pearson correlation coefficient, and uses the mutual information ($I[x_i, x_j]$) estimator of Kraskov *et al.* (*55*), which calculates the marginal entropy ($H[x_i]$ and $H[x_j]$) and joint entropy ($H[x_i, x_j]$) using k-nearest neighbor (k-NN) algorithm

$$I[x_i, x_j] = H[x_i] + H[x_j] - H[x_i, x_j]$$

where x_i and x_j define the positional fluctuation vectors of atoms i and j, respectively. The r_{MI} can be defined as

$$r_{MI}[x_i, x_j] = \{1 - \exp(-2I[x_i, x_j]/d)\}^{-1/2}$$

where $r_{MI}[x_i, x_j]$ are mutual information–based generalized correlation coefficient for variables x_i and x_j and have a value 0 for fully uncorrelated (independent) variables and may have a value up to 1 for correlated variables (*54*); d is the dimensionality of the variable x.

Principal component analysis

PCA is a technique to reduce the multidimensional motions in proteins, resulting from the simulations and in the biologically relevant larger global motions (*56*). In PCA, a "$3m \times 3m$" C-matrix (covariance matrix) from the atomic positions is generated for Cα residues, where m represents the number of residues considered for the analysis. By applying eigen decomposition to this C-matrix, a $3m$ set of eigenvectors corresponding to modes (*57*) was generated and the top two eigenvectors were considered for analysis. The 1-μs simulation trajectory of PurL with glutamine was analyzed to get the principal modes of motion in different protein domains. The analysis was performed using g_covar and g_anaeig utilities of ROMACS (*48*).

SUPPLEMENTARY MATERIALS

Supplementary material for this article is available at http://advances.sciencemag.org/cgi/content/full/6/14/eaay7919/DC1

View/request a protocol for this paper from *Bio-protocol*.

REFERENCES AND NOTES

1. J.-P. Changeux, S. J. Edelstein, Allosteric mechanisms of signal transduction. *Science* **308**, 1424–1428 (2005).
2. K. Gunasekaran, B. Ma, R. Nussinov, Is allostery an intrinsic property of all dynamic proteins? *Proteins* **57**, 433–443 (2004).
3. N. M. Goodey, S. J. Benkovic, Allosteric regulation and catalysis emerge via a common route. *Nat. Chem. Biol.* **4**, 474–482 (2008).
4. K. Henzler-Wildman, D. Kern, Dynamic personalities of proteins. *Nature* **450**, 964–972 (2007).
5. D. E. Koshland Jr., Conformational changes: How small is big enough? *Nat. Med.* **4**, 1112–1114 (1998).
6. H. N. Motlagh, J. O. Wrabl, J. Li, V. J. Hilser, The ensemble nature of allostery. *Nature* **508**, 331–339 (2014).
7. D. D. Boehr, D. McElheny, H. J. Dyson, P. E. Wright, The dynamic energy landscape of dihydrofolate reductase catalysis. *Science* **313**, 1638–1642 (2006).
8. S.-R. Tzeng, C. G. Kalodimos, Allosteric inhibition through suppression of transient conformational states. *Nat. Chem. Biol.* **9**, 462–465 (2013).
9. A. Gora, J. Brezovsky, J. Damborsky, Gates of enzymes. *Chem. Rev.* **113**, 5871–5923 (2013).
10. B. W. Miles, F. M. Raushel, Synchronization of the three reaction centers within carbamoyl phosphate synthetase. *Biochemistry* **39**, 5051–5056 (2000).
11. R. H. H. van den Heuvel, D. I. Svergun, M. V. Petoukhov, A. Coda, B. Curti, S. Ravasio, M. A. Vanoni, A. Mattevi, The active conformation of glutamate synthase and its binding to ferredoxin. *J. Mol. Biol.* **330**, 113–128 (2003).
12. Y. Fan, L. Lund, Q. Shao, Y.-Q. Gao, F. M. Raushel, A combined theoretical and experimental study of the ammonia tunnel in carbamoyl phosphate synthetase. *J. Am. Chem. Soc.* **131**, 10211–10219 (2009).
13. B. N. Chaudhuri, S. C. Lange, R. S. Myers, S. V. Chittur, V. J. Davisson, J. L. Smith, Crystal structure of imidazole glycerol phosphate synthase: A tunnel through a (β/α)8 barrel joins two active sites. *Structure* **9**, 987–997 (2001).
14. T. Mukherjee, J. Hanes, I. Tews, S. E. Ealick, T. P. Begley, Pyridoxal phosphate: Biosynthesis and catabolism. *Biochim. Biophys. Acta.* **1814**, 1585–1596 (2011).
15. J. H. Kim, J. M. Krahn, D. R. Tomchick, J. L. Smith, H. Zalkin, Structure and function of the glutamine phosphoribosylpyrophosphate amidotransferase glutamine site and communication with the phosphoribosylpyrophosphate site. *J. Biol. Chem.* **271**, 15549–15557 (1996).
16. S. Mouilleron, M.-A. Badet-Denisot, B. Badet, B. Golinelli-Pimpaneau, Dynamics of glucosamine-6-phosphate synthase catalysis. *Arch. Biochem. Biophys.* **505**, 1–12 (2011).

17. R. Anand, A. A. Hoskins, J. Stubbe, S. E. Ealick, Domain organization of Salmonella typhimurium formylglycinamide ribonucleotide amidotransferase revealed by X-ray crystallography. *Biochemistry* **43**, 10328–10342 (2004).
18. A. A. Hoskins, R. Anand, S. E. Ealick, J. Stubbe, The formylglycinamide ribonucleotide amidotransferase complex from Bacillus subtilis: Metabolite-mediated complex formation. *Biochemistry* **43**, 10314–10327 (2004).
19. Y. Zhang, M. Morar, S. E. Ealick, Structural biology of the purine biosynthetic pathway. *Cell. Mol. Life Sci.* **65**, 3699–3724 (2008).
20. J. M. Krahn, J. H. Kim, M. R. Burns, R. J. Parry, H. Zalkin, J. L. Smith, Coupled formation of an amidotransferase interdomain ammonia channel and a phosphoribosyltransferase active site. *Biochemistry* **36**, 11061–11068 (1997).
21. I. Rivalta, M. M. Sultan, N.-S. Lee, G. A. Manley, J. P. Loria, V. S. Batista, Allosteric pathways in imidazole glycerol phosphate synthase. *Proc. Natl. Acad. Sci. U.S.A.* **109**, E1428–E1436 (2012).
22. S. Mouilleron, M.-A. Badet-Denisot, B. Golinelli-Pimpaneau, Glutamine binding opens the ammonia channel and activates glucosamine-6P synthase. *J. Biol. Chem.* **281**, 4404–4412 (2006).
23. R. Anand, A. A. Hoskins, E. M. Bennett, M. D. Sintchak, J. A. Stubbe, S. E. Ealick, A model for the Bacillus subtilis formylglycinamide ribonucleotide amidotransferase multiprotein complex. *Biochemistry* **43**, 10343–10352 (2004).
24. M. Morar, R. Anand, A. A. Hoskins, J. Stubbe, S. E. Ealick, Complexed structures of formylglycinamide ribonucleotide amidotransferase from *Thermotoga maritima* describe a novel atp binding protein superfamily. *Biochemistry* **45**, 14880–14895 (2006).
25. L. Ballut, S. Violot, S. Shivakumaraswamy, L. P. Thota, M. Sathya, J. Kunala, B. W. Dijkstra, R. Terreux, R. Haser, H. Balaram, N. Aghajari, Active site coupling in Plasmodium falciparum GMP synthetase is triggered by domain rotation. *Nat. Commun.* **6**, 8930 (2015).
26. F. Massière, M. A. Badet-Denisot, The mechanism of glutamine-dependent amidotransferases. *Cell. Mol. Life Sci.* **54**, 205–222 (1998).
27. A. S. Tanwar, D. J. Sindhikara, F. Hirata, R. Anand, Determination of the formylglycinamide ribonucleotide amidotransferase ammonia pathway by combining 3D-RISM theory with experiment. *ACS Chem. Biol.* **10**, 698–704 (2015).
28. R. G. Parra, N. P. Schafer, L. G. Radusky, M.-Y. Tsai, A. B. Guzovsky, P. G. Wolynes, D. U. Ferreiro, Protein frustratometer 2: A tool to localize energetic frustration in protein molecules, now with electrostatics. *Nucleic Acids Res.* **44** (W1), W356–W360 (2016).
29. J.-L. Risler, P. Brézellec, S. Pasek, Gene fusion/fission is a major contributor to evolution of multi-domain bacterial proteins. *Bioinformatics* **22**, 1418–1423 (2006).
30. L. Dossena, B. Curti, M. A. Vanoni, Activation and coupling of the glutaminase and synthase reaction of glutamate synthase is mediated by E1013 of the ferredoxin-dependent enzyme, belonging to loop 4 of the synthase domain. *Biochemistry* **46**, 4473–4485 (2007).
31. S. M. Cuesta, S. A. Rahman, N. Furnham, J. M. Thornton, The classification and evolution of enzyme function. *Biophys. J.* **109**, 1082–1086 (2015).
32. J. A. Endrizzi, H. Kim, P. M. Anderson, E. P. Baldwin, Crystal structure of Escherichia coli cytidine triphosphate synthetase, a nucleotide-regulated glutamine amidotransferase/ATP-dependent amidoligase fusion protein and homologue of anticancer and antiparasitic arug targets. *Biochemistry* **43**, 6447–6463 (2004).
33. F. List, M. C. Vega, A. Razeto, M. C. Häger, R. Sterner, M. Wilmanns, Catalysis uncoupling in a glutamine amidotransferase bienzyme by unblocking the glutaminase active site. *Chem. Biol.* **19**, 1589–1599 (2012).
34. O. Pantoja, High affinity ammonium transporters: Molecular mechanism of action. *Front. Plant Sci.* **3**, 34 (2012).
35. M. Landau, I. Mayrose, Y. Rosenberg, F. Glaser, E. Martz, T. Pupko, N. Ben-Tal, ConSurf 2005: The projection of evolutionary conservation scores of residues on protein structures. *Nucleic Acids Res.* **33**, W299–W302 (2005).
36. A. S. Tanwar, V. D. Goyal, D. Choudhary, S. Panjikar, R. Anand, Importance of hydrophobic cavities in allosteric regulation of formylglycinamide synthetase: Insight from xenon trapping and statistical coupling analysis. *PLOS ONE* **8**, e77781 (2013).
37. F. J. Schendel, J. Stubbe, Substrate specificity of formylglycinamidine synthetase. *Biochemistry* **25**, 2256–2264 (1986).
38. E. Bernt, H. U. Bergmeyer, L-Glutamate UV-assay with gutamate dehydrogenase and NAD, in *Methods of Enzymatic Analysis (Second Edition)*, H. U. Bergmeyer, Ed. (Academic Press, 1974), pp. 1704–1715.
39. F. Salinas, A. E. Mansilla, J. J. B. Nevado, Derivative spectrophotometric determination of sulphonamides by the Bratton-Marshall reaction. *Anal. Chim. Acta* **233**, 289–294 (1990).
40. Z. Otwinowski, W. Minor, Processing of X-ray diffraction data collected in oscillation mode, in *Methods in Enzymology* (Academic Press, 1997), vol. 276, pp. 307–326.
41. W. Kabsch, Integration, scaling, space-group assignment and post-refinement. *Acta Crystallogr. D Biol. Crystallogr.* **66**, 133–144 (2010).
42. A. J. McCoy, R. W. Grosse-Kunstleve, P. D. Adams, M. D. Winn, L. C. Storoni, R. J. Read, Phaser crystallographic software. *J. Appl. Cryst.* **40**, 658–674 (2007).
43. S. Panjikar, V. Parthasarathy, V. S. Lamzin, M. S. Weiss, P. A. Tucker, On the combination of molecular replacement and single-wavelength anomalous diffraction phasing for automated structure determination. *Acta Crystallogr. D Biol. Crystallogr.* **65**, 1089–1097 (2009).
44. A. A. Vagin, R. A. Steiner, A. A. Lebedev, L. Potterton, S. McNicholas, F. Long, G. N. Murshudov, REFMAC5 dictionary: Organization of prior chemical knowledge and guidelines for its use. *Acta Crystallogr. D Biol. Crystallogr.* **60**, 2184–2195 (2004).
45. M. D. Winn, C. C. Ballard, K. D. Cowtan, E. J. Dodson, P. Emsley, P. R. Evans, R. M. Keegan, E. B. Krissinel, A. G. W. Leslie, A. McCoy, S. J. McNicholas, G. N. Murshudov, N. S. Pannu, E. A. Potterton, H. R. Powell, R. J. Read, A. Vagin, K. S. Wilson, Overview of the CCP4 suite and current developments. *Acta Crystallogr. D Biol. Crystallogr.* **67**, 235–242 (2011).
46. P. Emsley, B. Lohkamp, W. G. Scott, K. Cowtan, Features and development of Coot. *Acta. Crystallogr. D Biol. Crystallogr.* **66**, 486–501 (2010).
47. A. D. MacKerell Jr., M. Feig, C. L. Brooks III, Improved treatment of the protein backbone in empirical force fields. *J. Am. Chem. Soc.* **126**, 698–699 (2004).
48. H. J. C. Berendsen, D. van der Spoel, R. van Drunen, GROMACS: A message-passing parallel molecular dynamics implementation. *Comput. Phys. Commun.* **91**, 43–56 (1995).
49. W. L. Jorgensen, J. Chandrasekhar, J. D. Madura, R. W. Impey, M. L. Klein, Comparison of simple potential functions for simulating liquid water. *J. Chem. Phys.* **79**, 926–935 (1983).
50. H. J. C. Berendsen, J. P. M. Postma, W. F. van Gunsteren, A. DiNola, J. R. Haak, Molecular dynamics with coupling to an external bath. *J. Chem. Phys.* **81**, 3684–3690 (1984).
51. G. Bussi, D. Donadio, M. Parrinello, Canonical sampling through velocity rescaling. *J. Chem. Phys.* **126**, 014101 (2007).
52. M. Parrinello, A. Rahman, Polymorphic transitions in single crystals: A new molecular dynamics method. *J. Appl. Phys.* **52**, 7182–7190 (1981).
53. P. Hünenberger, A. E. Mark, W. F. Van Gunsteren, Fluctuation and cross-correlation analysis of protein motions observed in nanosecond molecular dynamics simulations. *J. Mol. Biol.* **252**, 492–503 (1995).
54. O. F. Lange, H. Grubmüller, Generalized correlation for biomolecular dynamics. *Proteins* **62**, 1053–1061 (2006).
55. A. Kraskov, H. Stögbauer, P. Grassberger, Estimating mutual information. *Phys. Rev. E* **69**, 066138 (2004).
56. G. G. Maisuradze, A. Liwo, H. A. Scheraga, Principal component analysis for protein folding dynamics. *J. Mol. Biol.* **385**, 312–329 (2009).
57. C. C. David, D. J. Jacobs, Principal component analysis: A method for determining the essential dynamics of proteins. *Methods Mol. Biol.* **1084**, 193–226 (2014).

Acknowledgments: We thank A. Chowdhury, R. B. Sunoj, S. Kar, and Pradeepkumar P.I. for their helpful suggestions to improve the manuscript. We thank the XRD facility IIT Bombay and beamline ID29, European Synchrotron Radiation Facility (ESRF), Grenoble, France, for initial crystallization screening and crystallographic data collection. We also thank J. Stubbe (Massachusetts Institute of Technology, USA) for gifting FGAR. **Funding:** This work was funded by Indo-South Africa Joint Science and Technology Research Cooperation Grant awarded by the Department of Science and Technology, Government of India (grant number DST/INT/SOUTH AFRICA/P-04/2014) and the National Research Foundation (NRF) of South Africa (grant number 90702). J.M. would like to acknowledge the computing facilities at TIFR Hyderabad developed using intramural research grant received from TIFR, India via the Department of Atomic Energy (DAE), Ramanujan Fellowship and Research funds provided by Department of Science and Technology (DST) of India (CRG/2019/001219). **Author contributions:** Designed research: N.S. and R.A.; performed research: N.S., N.A., P.S., and J.M.; analyzed data: N.S., N.A., P.S., J.M., and R.A.; wrote the manuscript: R.A. and N.S.; contributed to substrate production efforts and critically edited the manuscript for content and clarity: E.S. **Competing interests:** The authors declare that they have no competing interests. **Data and materials availability:** All the newly solved crystal structures reported here are available in RSCB PDB under accession numbers 6JT7, 6JT8, 6JT9, and 6JTA. All data needed to evaluate the conclusions in the paper are present in the paper and/or the Supplementary Materials. Additional data related to this paper may be requested from the authors.

Submitted 18 July 2019
Accepted 8 January 2020
Published 3 April 2020
10.1126/sciadv.aay7919

Citation: N. Sharma, N. Ahalawat, P. Sandhu, E. Strauss, J. Mondal, R. Anand, Role of allosteric switches and adaptor domains in long-distance cross-talk and transient tunnel formation. *Sci. Adv.* **6**, eaay7919 (2020).